batteries

MDPI

Article

Selective Separation of Lithium from Leachate of Spent Lithium-Ion Batteries by Zirconium Phosphate/Polyacrylonitrile Composite: Leaching and Sorption Behavior

Baffa Haruna [1,2], Zhongyan Luo [1], Mujtaba Aminu Muhammad [1,2], Jinfeng Tang [3,*], Jukka Kuva [4], Risto Koivula [5], Hongli Bao [1,2] and Junhua Xu [1,2,4,5,*]

1 Fujian Institute of Research on the Structure of Matter, Chinese Academy of Sciences, Fuzhou 350002, China; baffaharuna@fjirsm.ac.cn (B.H.); luozhongyan@fjirsm.ac.cn (Z.L.); ameen93@fjirsm.ac.cn (M.A.M.); hlbao@fjirsm.ac.cn (H.B.)
2 Chinese Academy of Sciences University, Beijing 100049, China
3 Linköping University—Guangzhou University Research Center on Urban Sustainable Development, School of Environmental Science and Engineering, Guangzhou University, Guangzhou 510006, China
4 Geological Survey of Finland, P.O. Box 96, FI-02151 Espoo, Finland; jukka.kuva@gtk.fi
5 Department of Chemistry-Radiochemistry, University of Helsinki, P.O. Box 55, FI-00014 Helsinki, Finland; risto.koivula@helsinki.fi
* Correspondence: jinfeng@gzhu.edu.cn (J.T.); junhua.xu@gtk.fi (J.X.)

Abstract: This study introduces a straightforward and effective amorphous ZrP/polyacrylonitrile composite ion exchange method for separating Li from the leachate of spent Li-ion batteries (NMC 111). The cathode materials were leached with a series of optimized experiments. The influence of operating variables, including the H_2SO_4 concentration, temperature, H_2O_2 concentration, and pulp density, on leaching efficiency was examined to determine the optimal conditions for sorption experiments. The leaching efficiencies of Li, Co, Ni, and Mn were found to be 99.9%, 99.5%, 98.8%, and 99.9%, respectively. Subsequently, batch sorption experiments were performed by using am-ZrP/PAN, including the determination of the effect of pH, sorption kinetics, and the sorption isotherm. The effect of pH on adsorption was examined in 1 mmol/L equimolar solutions of Li, Ni, Mn, and Co. Li was separated from Mn, Co, and Ni in the leaching liquor. The adsorbent for Mn, Co, and Ni sorption better fitted pseudo-second-order kinetics. High selectivity for Li was observed, even at the higher solution concentration of 15 mM Li, Ni, Co and Mn. In addition, the column loading process demonstrated selectivity for Li over Co, Ni, and Mn metal ions. The preliminary evaluation of the whole process with mass flow demonstrated that it would be feasible to achieve full separation and metal recovery by integrating a combined hydrometallurgical method in future studies. However, much work is still needed to develop a practical separation flowsheet.

Keywords: spent lithium-ion batteries; leaching; am-ZrP/PAN; sorption; separation

Citation: Haruna, B.; Luo, Z.; Muhammad, M.A.; Tang, J.; Kuva, J.; Koivula, R.; Bao, H.; Xu, J. Selective Separation of Lithium from Leachate of Spent Lithium-Ion Batteries by Zirconium Phosphate/Polyacrylonitrile Composite: Leaching and Sorption Behavior. *Batteries* **2024**, *10*, 254. https://doi.org/10.3390/batteries10070254

Academic Editor: Stefan Adams

Received: 21 May 2024
Revised: 8 July 2024
Accepted: 12 July 2024
Published: 17 July 2024

1. Introduction

In recent years, the demand for lithium-ion batteries (LIBs) has constantly increased due to their use in energy storage devices and various types of portable equipment, such as cell phones and personal computers [1–3]. In these batteries, the use of lithium (Li), nickel (Ni), cobalt (Co) and manganese (Mn) oxides (NMC) has become customary because of the advantage of high specific energy [4–6]. A typical mixed cathode of LIBs (NMC) contains critical metals such as Li, Ni, Mn, and Co, which is of economic concern due to future supply chain risks [7]. Apart from the economic point of view, improper disposal of end-of-life batteries results in environmental problems. Several research groups have reported potential impacts of transition metals on environmental and human health [8–10]. However, the significant quantities of metals contained in end-of-life LIBs could, if recycled, become a secondary source to address the shortage of these metals [7,11]. Therefore,

developing a sustainable and efficient method for recycling these metals from end-of-life LIBs is highly desirable.

Currently, hydrometallurgy, biometallurgy, and pyrometallurgy are the most widely used processes for the treatment of end-of-life LIBs [12–14]. Among these, hydrometallurgy has become the most researched process due to its low energy consumption [15,16]. Leaching is an important step in hydrometallurgy to dissolve valuable metals from the cathode powder of spent LIBs using organic or inorganic acids such as sulfuric acid, hydrochloric acid, tartaric acid, and nitric acid [17,18], and the metals are then separated from the leachate by precipitation, solvent extraction, ion exchange, or a combination of these techniques [19–21]. The precipitation process has a low yield of the target metal because of the co-precipitation of other highly concentrated metals, and it is also time-consuming. In solvent extraction, the organophosphorus extractants include PC88A (2-ethylhexylphosphonic acid mono-2-ethyl-hexyl ester), Cyanex 272 (di-isooctyl phosphonic acid), and D2EHPA (di-2-ethylhexyl phosphoric acid). Although these extractants are commercially available, the use of volatile and flammable dilutants such as kerosene, which are environmental pollutants, is required. In addition, for end-of-life LIB cathodes, which contain Li, Co, Mn, and Ni, multiple extractants are used to recover the target metals, and they tend to cause the loss of transition metals [22–25]. For example, D2EHP as an extraction agent can help separate Co, Ni, and Mn from Li, but can cause a loss of metals [26]. Furthermore, the product of these treatments is a mixed solution of different extractants and organic or inorganic chemicals, and countless separation stages and pH adjustments are needed to obtain the metals from the leachate.

The current traditional recovery methods place emphasis on the extraction of transition metals (Co, Ni, and Mn), but is difficult to separate them from each other. This also tends to cause the severe loss of metal ions due to the use of multiple extraction stages to separate them [27,28]. Manganese, nickel, and cobalt are considered as elements of the same type due to their similar physical and chemical properties. Thus, separating them from lithium could be a more attractive approach, as the mixture can be directly used to prepare ternary material precursors [26,29], or to separate cobalt, manganese, and nickel, it can be used to prepare cobalt sulfate, manganese sulfate, and nickel sulfate without Li impurities [30,31]. For instance, Yue et al. [32] proposed that the co-extraction of transition metals from the leachate of spent LIBs with neodecanoic acid could avoid the loss of metals that occurs during the traditional process of separating metals one by one. Their results revealed that the extraction efficiency of Mn, Ni, and Co could reach 97.05%, 99.18%, and 98.47%, respectively.

Although remarkable results have been achieved, less attention has been paid to the recycling of the extractant, as the method consists of two extraction steps, primary and secondary extraction, which is of great interest for practical use. An inorganic ion exchanger has been employed in the purification of metal ions and adsorption as an alternative method to solvent extraction to obtain high purity fractions due to its high selectivity, ease of operation, reusability, and resistance to radiation [33–35]. Existing methods are challenged by their adsorption capacities for leachate transition metals (Co, Ni, Mn), which makes it difficult to separate them from lithium. For example, lithium-ion sieves can separate lithium from a ternary solution (Li, Co, and Ni) after five adsorption–desorption cycles. It has been reported that about 92% Li, 66% Ni, and 11% Co were recovered, while almost 34% of Ni and 89% of Co were lost due to the relatively low selectivity of the adsorbent [36]. Lister et al. [37] applied Dowex M4195 resin as an absorbent to separate transition metals from lithium. According to their experimental results, approximately 87% of Ni and 59% of Co were eluted, and no separation between Li and Mn was achieved using continuous flows. Sami et al. [38] also proposed the removal of Mn from a leachate solution using Lewatit TP260, whereby Li–Ni–Co as the targeted precursor is left in raffinate, which is a mixture of Li, Ni, Co, and a byproduct. However, to the best of our knowledge, although these methods have achieved some success, the highly efficient selectively separation of Li from a solution of Li, Ni, Co, and Mn requires further investigation. Considering this topic

from the perspective of reverse thinking, the recovery of ternary Co, Ni, and Mn metals from spent lithium leachate containing Li, Ni, Co, and Mn via sorption is a challenging and important task, but a good option to achieve their separation. It appears that the strategy of adsorption using a suitable sorbent that can selectively adsorb Co, Ni, and Mn from the leachate (NMC) could address various issues, such as reducing the number of separation stages/extractants in the process and/or eliminating the use of a highly toxic dilutant, minimizing the loss of transition metals, and reducing the ecological impact.

Inspired by previous research, we conducted a leaching experiment on the cathode powder of end-of-life LIBs (NMC 111). Considering the low leaching efficiency of end-of-life LIBs (NMC 111) at a high pulp density, we commenced leaching experiments to obtain a high concentration of the cathodic material in the acid leaching solution, and only important parameters such as the H_2SO_4 concentration, temperature, H_2O_2 concentration, pulp density, and time were investigated. For Li separation, a simple and efficient method was demonstrated in which Co, Mn, and Ni were adsorbed from end-of-life LIBs (NMC) using am-ZrP/polyacrylonitrile (am-ZrP/PAN) and were separated from Li. To predict the possibility of separation, the ion exchange batch experiment examined the effect of pH, the kinetics equilibrium, isothermal sorption and column test experiment separation were performed for further separation (Figure 1).

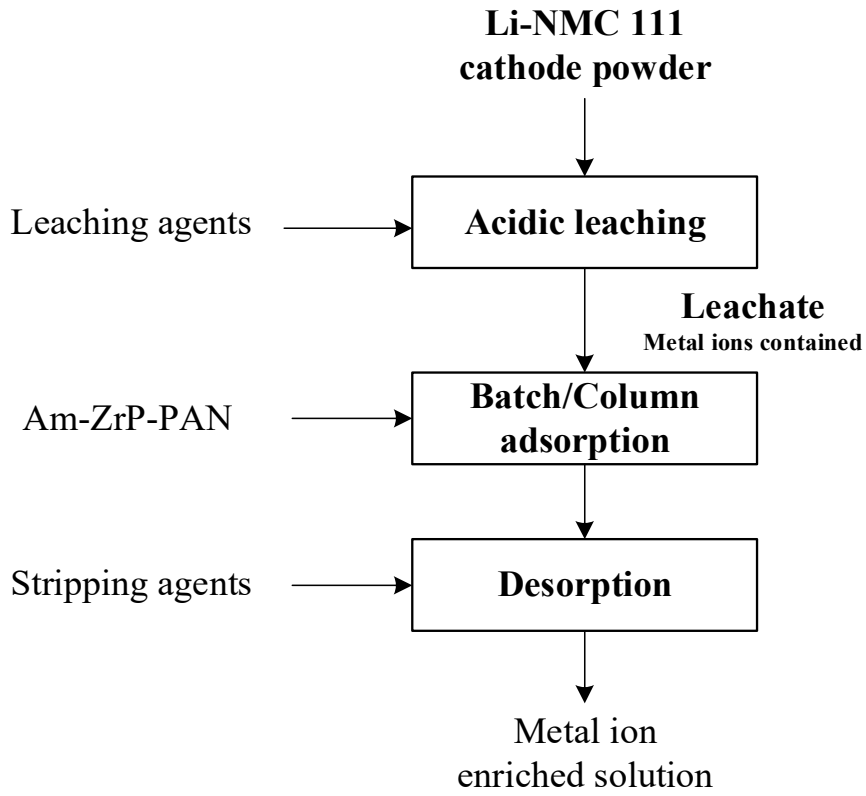

Figure 1. Scheme of the proposed method for the leaching, batch sorption, and corresponding column experiments on NMC 111 cathode metals from end-of-life lithium-ion batteries.

2. Experimental

2.1. Chemicals

Lithium sulfate monohydrate (99%+) was purchased from Damas-beta, nickel (II) sulfate hexahydrate (98%), nitric acid (65–68%), sulfuric acid (98%), hydrogen peroxide 30% aqueous solution, and sodium hydroxide 96% from Sinopharm Chemical Reagent (Shanghai, China), cobalt sulfate heptahydrate (99%) and manganese sulfate monohydrate (99%) from Aladdin, polyacrylonitrile (PAN) (average Mw 150,000), dimethylformamide (>99.9%), Tween® 80, and zirconium tetrachloride (>99.9%) from Sigma-Aldrich (St. Louis,

MO, USA), Li-ion battery cathode powder (NMC 1:1:1), model SN1B, batch number 0012008, was purchased from Shenzhen Kejing Star Technology Company (Shenzhen, China), and water from MTI. Milli-Q® water (18.2 MΩ) (Merck, Rahway, NJ, USA) was used. All chemicals were used as received, without further purification.

2.2. Characterization

A field emission scanning electron microscope (FESEM) (SU-8010, Tokyo, Japan) and a Hitachi SU3500 scanning electron microscope were used for characterization. X-ray powder diffraction (XRD) patterns were recorded using a MiniFlex600 X-ray powder diffractometer operating at a potential of 40 kV and a current of 40 mA, with Cu-Kα (λ = 1.542) radiation. X-ray computed tomography (XCT) analysis was performed with a GE Phoenix v | tome | x s 240 using a 180 kV/15 W nanofocus tube with a 60 kV accelerating voltage and a 410 µA current, resulting in a tube power of 24.6 W with the second smallest focus mode. In total, 2700 projections were taken during a 360° rotation. At each angle, the detector waited for a single exposure time and then took an average over three exposures. With a single exposure time of 2000 ms, the total scan time was thus six hours. Reconstruction was performed with ring artifact reduction but without beam hardening correction. The resulting spatial resolution was 1.19 µm. The images were analyzed using ThermoFisher PerGeos 2020.2. A Mettler Toledo pH meter (FG2/EL2) was used to measure pH values. Thermogravimetry (TG) was applied with a Metter Toledo TGA850 in N_2 flow with a heating rate of 10 °C min^{-1}. The concentrations of Li, Co, Ni, and Mn in the solutions were determined by inductively coupled plasma-atomic emission spectrometry (ICP-AES, Perkin Elmer Avio200, Waltham, MA, USA).

2.3. Synthesis of am-ZrP/PAN

Am-ZrP material was prepared according to a previously published method [39]. Briefly, 400 mL of 1.25 M phosphoric acid (H_3PO_4) was added to a mixture of 30.7 g of zirconium tetrachloride ($ZrCl_4$) and 430 mL of 2 M hydrochloric acid (HCl). The formed precipitate was left in the mother solution overnight. After phase separation, the full conversion of the materials to H-forms was achieved by treating the precipitates with 1 L of 1 M nitric acid (HNO_3). Finally, the product was washed with water until pH 3 and air-dried at 60 °C for 2 days. The am-ZrP/PAN composite was then prepared. First, 7.2 g of am-ZrP and 2 mL of Tween® 80 were mixed with 84 mL of N, N-dimethylformamide (DMF) at 60 °C for 2 h by magnetic stirring to obtain a homogeneous solution. Then, 4.8 g of PAN was added to the solution and continuously stirred for another 2 h. The gelled composite beads were obtained by dripping the mixture into deionized water using a needle with a 0.6 mm diameter.

2.4. Leaching Procedure

All leaching experiments were conducted using a 250 mL glass reactor placed in a water bath with a magnetic stirrer and a temperature controller, and the reactor was covered to avoid water loss. The effect of various reaction parameters, such as the H_2SO_4 concentration (0.5–2.5 M), temperature (25–90 °C), H_2O_2 concentration (0.0–2.0%), pulp density (10–100 g/L), and time (0.25–72 h), were investigated at a fixed stirring speed of 650 rpm. After leaching, the insoluble residues were separated from the leachate via filtration and then washed and dried at 60 °C. The $LiNi_{1/3}Co_{1/3}Mn_{1/3}O_2$ cathode material was dissolved in aqua regia (HCl to HNO_3 ratio 3:1) to enable the analysis of its metal content. The metal contents were found to be 7.80% Li, 19.24% Mn, 20.71% Co, and 21.06% Ni. The leaching efficiency of Li, Co, Ni, and Mn could be calculated according to Equation (1).

$$\text{Leaching efficiency} = \frac{\text{Metal content in leachate}}{\text{Total amount of metal in cathodic materials}} \times 100\%. \quad (1)$$

2.5. Effect of pH on Metal Uptake

The effect of pH on metal uptake by am-ZrP/PAN was examined over a pH range of 1–5 at 298 K. Typically, 50 mg of am-ZrP/PAN was placed in a glass vial and 20 mL of a 1 mM equimolar solution of Li, Co, Ni, and Mn was added and equilibrated in a rotary mixer (60 rpm) for three days. After equilibration, the pH values and metal concentrations of the supernatant solution were measured.

The adsorption capacity (q_e) is defined as the amount of metals sorbed onto the adsorbent (mg g^{-1}), and the distribution coefficient k_d can be described as the distribution of metal ions between the concentration solution and adsorbent. They were calculated from Equations (2) and (3), respectively.

$$q_e = \frac{(C_i - C_e)V}{m} \quad (2)$$

and

$$k_d = \frac{(C_i - C_e)V}{C_e m} \quad (3)$$

where C_i is the initial metal concentration in the solution (mg L^{-1}), Ce is the equilibrium concentration of metal ions in the solution (mg L^{-1}), V is the volume of the solution (L), and m is the mass of the adsorbent (g).

2.6. Adsorption Kinetics Studies

Adsorption kinetics were investigated under varying reaction times (from 0.25 to 72 h), with 50 mg of am-ZrP/PAN being placed in a glass vial with 20 mL of a 1 mM equimolar solution of Li, Co, Ni, and Mn at pH 2.5. The concentration of the metals in the supernatant solution was measured using ICP-AES.

2.7. Isotherm Studies

Fifty milligrams of am-ZrP/PAN was placed in a glass vial with 20 mL of a solution of Li, Co, Ni, and Mn at varying concentrations (1.0–20 mM, with a sufficient interval) and was equilibrated at pH 2.5 for three days in a rotary mixer (60 rpm). The concentration of the metals in the supernatant solution was measured using ICP-AES.

2.8. Column Chromatography Experiments

Column chromatography experiments were conducted in Bio-Rad glass columns of 100 mm height with an inner diameter of 10 mm at room temperature (298 K), with 1.0 g of am-ZrP/PAN being carefully packed into the columns. The breakthrough curves were studied by pumping the leachate solution from the end-of-life NMC with a feed concentration of approximately 48.7 ppm Co, 46 ppm Mn, 50.0 ppm Ni, and 19.0 ppm Li at approximately pH 2.5. All column chromatography studies were conducted at 2 bed volumes (BV) per 1 h speed.

The recovery of metals from leachate NMC 111 by the am-ZrP/PAN columns was calculated by applying Equation (4).

$$\text{Recovery}(\%) = \frac{C_i - C_L}{C_i} \times 100 \quad (4)$$

where C_i (mmol L^{-1}) is the initial concentration of metal ions in the leachate solution, and C_L is the concentration of metal ions in the fractions collected after elution from the am-ZrP/PAN columns.

3. Results and Discussion

3.1. Characterization of am-ZrP/PAN

The beads of am-ZrP/PAN were characterized by FESEM, XCT, XRD, and TGA (Figure 2). The beads had a spherical shape and an average size of 2 mm. Surface imaging of the beads revealed internal porosity, which is desirable for stronger sorption (Figure 2a). The internal structure of the am-ZrP/PAN composite was examined by XCT. The image in Figure 2b illustrates the internal porosity of the beads. According to the analysis, the internal porosity, matrix, and density of the beads were about 50%, 47%, and 3%, respectively, indicating the high porosity of the am-Zrp/PAN. The bead of am-Zrp was characterized in our previous study [39,40]. As the main focus of the present study was on the separation of metals in solution, only typical characterizations of the obtained material were performed to check the properties. The XRD pattern in Figure 2c indicates a typical amorphous character for the am-ZrP phase, exhibiting some broad and low-intensity peaks at 10–70 degrees.

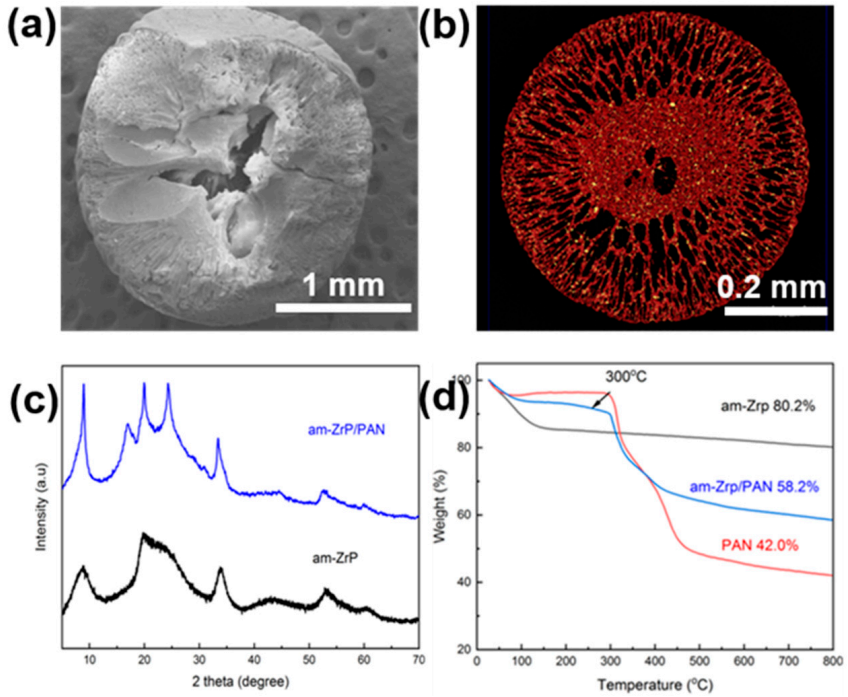

Figure 2. (**a**) SEM image of the surface of an am-ZrP/PAN bead. (**b**) XCT cross-section of one am-ZrP/PAN bead. (**c**) XRD pattern of the synthesized am-ZrP and am-ZrP/PAN. (**d**) TGA curves of the PAN beads, am-ZrP, and am-ZrP/PAN beads.

The TG curves of the am-Zrp, PAN beads, and am-Zrp/PAN beads are presented in Figure 2d. The weight loss of am-Zrp/PAN beads occurring below 300 °C can be attributed to the elimination of absorbed water, while the weight loss in the temperature range 300–800 °C can be attributed to the decomposition of H_2PO_4 functional groups of am-ZrP and PAN [41]. According to the thermal analysis above, the percentage of am-ZrP in the composite was calculated to be 42.7%.

3.2. Leaching Experiments

3.2.1. Effect of H_2SO_4 Concentration on Leaching Efficiency

The effect of the H_2SO_4 concentration on the leaching efficiencies for Li, Mn, Co, and Ni was examined under the conditions of 40 g/L pulp, 1.0% H_2O_2, and a leaching time of 1 h at 40 °C, as illustrated in Figure 3a. The leaching efficiencies for all the metals increased with an increase in the H_2SO_4 concentration from 0.5 to 2.5 M. When the concentration of H_2SO_4 reached 2.5 M, the leaching efficiencies were 97.4% for Li, 93.0% for Co, 93.3%

for Mn, and 95.8% for Ni. Therefore, 2.5 M was determined as the optimal concentration of H_2SO_4.

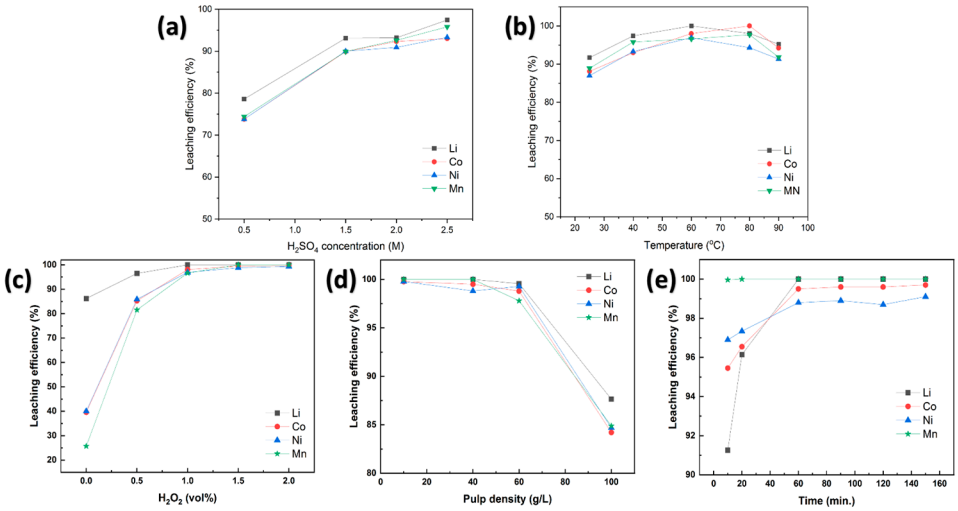

Figure 3. The effect of (**a**) H_2SO_4 concentration, (**b**) temperature, (**c**) H_2O_2 concentration, (**d**) pulp density, and (**e**) time on the leaching efficiencies for Co, Mn, Ni, and Li.

3.2.2. Effect of Temperature on Leaching Efficiency

The effect of temperature on the leaching efficiencies for Li, Mn, Co, and Ni was examined under the conditions of 40 g/L pulp, 1.0% H_2O_2, 2.5 M H_2SO_4, and a leaching time of 1 h, as illustrated in Figure 3b. The leaching efficiencies for Li, Co, Ni, and Mn were found to increase with an increase in temperature because metal leaching is an endothermic reaction. When the temperature was increased to 60 °C, the leaching efficiencies for Li, Co, Ni, and Mn were found to be 99.9%, 98.0%, 96.9%, and 96.6%, respectively. However, the leaching efficiencies for Li and Ni decreased, while those for Co and Mn slightly increased when the temperature was further increased to 80 °C. For example, the leaching efficiencies decreased from 99.9% to 98% for Li and from 96.9% to 94.3% for Ni, while they increased from 98% to 99.9% for Co and from 96.6% to 97.7% for Mn. The leaching efficiencies for all the metals drastically decreased when the temperature reached 90 °C. This was due to H_2O_2 decomposition when heated to a high temperature [42]. Therefore, 60 °C was determined to be the optimal temperature.

3.2.3. Effect of H_2O_2 Concentration on Leaching Efficiency

The effect of the H_2O_2 concentration on the leaching efficiencies for Li, Co, Ni, and Mn was examined under the conditions of 40 g/L pulp, 2.5 M H_2SO_4, and a leaching time of 1 h at 60 °C, as illustrated in Figure 3c. The leaching efficiencies for Li, Co, Ni, and Mn were found to be 86.2%, 39.5%, 39.9%, and 25.6% in the absence of H_2O_2. However, when 1.5% H_2O_2 was added, the leaching efficiencies increased to 99.7% for Li, 99.9% for Co, 99.9% for Ni, and 99.9% for Mn. The increase in the leaching efficiencies can be attributed to H_2O_2 acting as a reducing agent and accelerating the leaching reaction. The leaching efficiencies for all the metals remained nearly constant when the H_2O_2 concentration was further increased to 2.0%. Therefore, 1.5% was determined to be the optimal H_2O_2 concentration.

3.2.4. Effect of Pulp Density on Leaching Efficiency

The effect of pulp density on the leaching efficiencies for Li, Co, Ni, and Mn was examined under the conditions of 1.5% H_2O_2, 2.5 M H_2SO_4, and a leaching time of 1 h at 60 °C, as illustrated in Figure 3d. The results demonstrated nearly constant leaching efficiencies for Li, Co, Ni, and Mn in the pulp density range 10–40 g/L. However, the leaching efficiencies for all the metals drastically decreased when the pulp density was increased to more than 40 g/L. This was probably due to a decrease in the contact areas

between the solid and liquid, resulting in a decrease in the leaching reaction [43]. Therefore, 40 g/L was determined as the optimal pulp density.

3.2.5. Effect of Time on Leaching Efficiency

The effect of time on the leaching efficiencies for Li, Co, Ni, and Mn was examined under the conditions of 40 g/L pulp, 1.5% H_2O_2, and 2.5 M H_2SO_4 at 60 °C, as illustrated in Figure 3e. The leaching efficiencies for all the metals increased with increasing time. For instance, the leaching efficiencies for Li, Co, Ni, and Mn were 91.2%, 95.4%, 96.9%, and 99.9%, respectively, at 10 min. When the time was increased to 60 min, the leaching molar ratios of Li, Co, Ni, and Mn were 3.25: 1.00: 1.02: 1.01, respectively. In addition, the calculated leaching efficiencies for Li, Co, Ni, and Mn were found to be 99.9%, 99.5%, 98.8%, and 99.9%, respectively. However, the leaching efficiencies for all the metals were nearly constant over the time range from 60 to 150 min. Therefore, 60 min was selected as the optimal leaching time.

3.3. Sorption Experiments

3.3.1. Effect of pH on Adsorption

The effect of pH on the adsorption of Li, Co, Ni, and Mn was investigated with 1 mM solutions of Li, Co, Ni, and Mn over a broad pH range from 1 to 5 (Figure 4a). The adsorption of Co, Ni, and Mn increased with increasing pH, and no plateaus were observed in the adsorption curves due to hydrogen ions competing with other metal ions in ion exchange metal recovery. There was little or no metal uptake at approximately pH 1.0–2.0. This was most likely due to the inability of the ion exchanger to adsorb metals when the feed solution had a high H_2SO_4 concentration. The maximum adsorption values for Co, Ni, and Mn were obtained at approximately pH 5.0, being 19.01 mg g^{-1}, 15.29 mg g^{-1}, and 21.04 mg g^{-1}, respectively, while Li was left in the raffinate. The K_d values were lowest at pH 1–2, which was evident due to little or no adsorption onto the ion exchanger (Figure 4b). After this, the K_d values rapidly increased with an increase in pH. The maximum K_d values for individual metals were 2.8 × 10 mL g^{-1} for Li, 1.1 × 10^3 mL g^{-1} for Co, 5.5 × 10^2 mL g^{-1} for Ni, and 2.7 × 10^3 mL g^{-1} for Mn, which were obtained at pH 5.

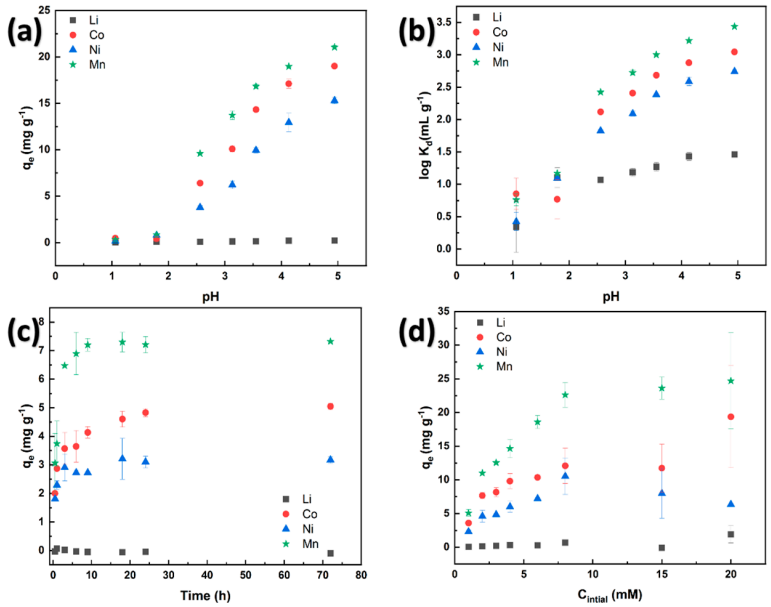

Figure 4. (**a**) The effect of pH on the absorption of Li, Co, Ni, and Mn by am-ZrP/PAN from a sulfuric acid solution with an initial metal concentration of 1 mM. (**b**) The K_d value at different pH values for am-ZrP/PAN. (**c**) The kinetics of Co, Mn, and Ni sorption by am-ZrP/PAN. Feed: Co = 1 mM, pH = 2.5, m = 0.05 g, V = 20 mL, mixing = 60 rpm at 298 K. (**d**) The sorption isotherms of Li, Co, Ni, and Mn in a sulfuric acid solution for am-ZrP/PAN adsorbent at a pH of 2.5.

3.3.2. Kinetics Study

The efficiency of an ion exchanger is defined by the reaction kinetics. The rate-determining step of ion exchange was investigated using pseudo-first-order, pseudo-second-order, and intra-particle diffusion equations

$$\log(q_e - q_t) = \log q_e - \left(\frac{k_1}{2.303}\right)t \quad (5)$$

and

$$\frac{t}{q_t} = \frac{1}{k_2 q_e^2} + \frac{1}{q_e}\,t, \quad (6)$$

where q_e and q_t are the amounts (mg g^{-1}) of metal ions at equilibrium and at time t, respectively, and (k_1 h^{-1}) and k_2 (mg g^{-1} h^{-1}) are the pseudo-first-order and pseudo-second-order rate constant models, respectively. q_t is determined by

$$q_{t\,=\,k_{int}t^{1/2}+C} \quad (7)$$

where K_{int} (mg g^{-1} $h^{-1/2}$) is the intra-particle diffusion constant, C (mg g^{-1}) is a constant proportional to the thickness of the boundary layer, and q_t (mg g^{-1}) is the concentration of metal ions in the ion exchanger at any given time.

The reaction kinetics of synthesized am-Zrp/PAN were evaluated in a 1 mM H_2SO_4 solution containing Li, Co, Ni, and Mn at pH 2.5 (Figure 4c). The uptakes for Co, Ni, and Mn had almost reached equilibrium at about 9 h. The kinetics of Co, Ni, and Mn were found to be faster than our previously studied equilibration time of 12 h for REE (dysprosium and neodymium) adsorption using am-Zrp/PAN [39]. This demonstrates the potential application of this ion exchanger to a more complex mixture of metal ions on a large scale.

The sorption of Co, Ni, and Mn ions by am-Zrp/PAN was better fitted by the pseudo-second-order kinetics model, with correlation coefficients of 0.993, 0.983, and 0.983 for Mn, Co, and Ni, respectively, than by the pseudo-first-order kinetics and intra-particle diffusion models (Table 1). This indicates that the adsorption mechanism may be chemical sorption rather than diffusion-related phenomena [33]. The results suggest that sorption appears to be a result of ion exchange between H^+, Mn^{2+}, Co^{2+}, and Ni^{2+}.

Table 1. Fitted pseudo-first-order and pseudo-second-order model parameters, and intra-particle diffusion for Li, Co, Ni, and Mn adsorption.

Metal Ion	$q_{max,epo.}$ (mmol g^{-1})	Pseudo-First-Order Kinetics			Pseudo-Second-Order Kinetics			Intra-Particle Diffusion		
		K_1 (h^{-1})	q_{eq} (mmol g^{-1})	R^2	K_2 (mg g^{-1} h^{-1})	q_{eq} (mmol g^{-1})	R^2	C (mg g^{-1})	$K_{ini.}$ (mg g^{-1} $h^{-1/2}$)	R^2
Co	0.045	0.101	0.047	0.976	0.095	0.045	0.983	0.107	0.065	0.882
Ni	0.037	0.006	0.017	0.997	0.015	0.037	0.989	0.121	0.055	0.814
Mn	0.095	0.060	0.176	0.976	0.015	0.095	0.993	0.027	0.013	0.933

3.3.3. Adsorption Isotherms

Adsorption isotherms were investigated at an equilibrium pH value of around 2.5. The adsorption of Co, Ni, and Mn increased with increasing concentrations of Li, Co, Ni, and Mn in the solution up to a concentration of approximately 8 mM (Figure 4d). At the highest solution concentration, Ni adsorption slightly decreased and Co adsorption increased, but the uptake of Mn was constant when comparing solution concentrations of 8 mM and 15 mM, which is evidently due to the consequential desorption and substitution of Ni by Co. However, the uptake values for Ni and Mn reached a plateau at a concentration of about 8 mM. The uptake values were 12.06 mg g^{-1} for Ni and 22.60 mg g^{-1} for Mn. In contrast, the maximum uptake of Co was 19.36 mg g^{-1} at a solution concentration of 20 mM. In summary, no Li uptake was observed, even at the higher concentration of 15 mM Li, Ni, Co and Mn.

3.4. Column Chromatography Loading and Desorption Studies

The separation of Co, Ni, and Mn from the leaching solution was examined with feed concentrations of 48.7 ppm Co, 46 ppm Mn, 50.0 ppm Ni, and 19.0 ppm Li at pH 2.5. In the column loading experiments, the column breakthrough curves for the adsorption of Li, Ni, Mn, and Co displayed similar adsorption behavior to the batch experiments, and no Li uptake was observed (Figure 5a). The metals exhibited a preference order of Mn, Co, Ni, and Li. Consequently, Li was the first to elute, with no uptake during loading, and the saturation time order for metals was recorded as Ni > Co > Mn. The loaded amounts of metal ions were calculated as 0.003 meq g^{-1} for Li, 0.061 meq g^{-1} for Ni, 0.123 meq g^{-1} for Co, and 0.170 meq g^{-1} for Mn. Therefore, a total of 0.357 meq g^{-1} ions were loaded in the fixed bed relative to the maximum loading of 100%.

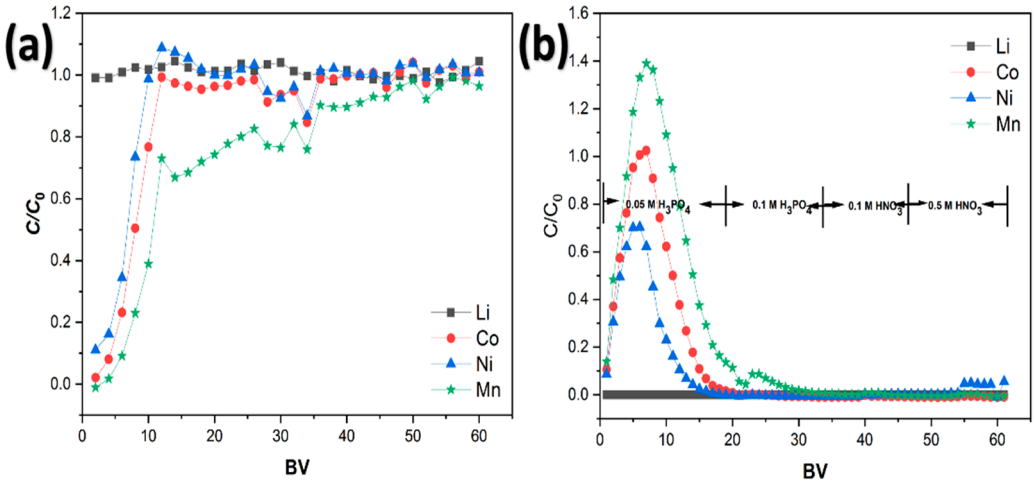

Figure 5. (**a**) Breakthrough curves for Li, Co, Ni, and Mn from the leachate solution of a spent lithium-ion battery at pH 2.5. Feed: Co 48.7 ppm, Mn 46 ppm, Ni 50.0 ppm, and Li 19.0 ppm. (**b**) Desorption curves for Li, Co, Ni, and Mn.

In the desorption experiments (Figure 5b), elution was performed with the series 0.05 M H_3PO_4, 0.1 M H_3PO_4, 0.1 HNO_3, and then finally with 0.5 M HNO_3. Desorption with 0.05 M H_3PO_4 resulted in modest separation of the metals in different BV. The calculated separation weight ratios of [Mn/Co], [Co/Ni], and [Mn/Ni] were 1.5, 1.7, and 2.6, respectively. One band appeared to be Mn, which was eluted as the concentration of H_3PO_4 increased to 0.1 M H_3PO_4. When employing 0.1 HNO_3 as the eluate, no metal was observed. Further increasing the concentration to 0.5 M HNO_3 resulted in the separation of a small amount of Ni. The column results demonstrated the high selectivity of Li over Co, Ni, and Mn metal ions, and that effective Li separation can be achieved during loading. However, the sorption capacity was low. Thus, it is crucial to increase the adsorption capacity to optimize the separation of metals.

3.5. Preliminary Evaluation of the Process

An integrated hydrometallurgical production flowsheet for recovering metals (Li, Mn, Co, Ni) from NMC 111 cathode materials in end-of-life lithium-ion batteries is presented here, with the mass flow illustrated in Figure 6. The process begins with a leaching stage designed to dissolve the targeted metals: Li, Co, Ni, and Mn. The resulting leachate is then processed through a sequential batch adsorption stage, in which Li is effectively and selectively captured using am-ZrP-PAN. Additionally, consistent outcomes can be achieved through column experiments. Subsequently, the ternary metal ions (Co, Ni, and Mn) are extracted in a batch process using an HNO_3 solution, yielding a solution enriched in metal ions. The recovery efficiency of the metal ions reached 99.1% for Co, 98.9% for Ni, and 97.8% for Mn. Considering the results of the overall batch experiments, it is feasible

to integrate metal recovery through a combined approach of leaching, adsorption, and solvent extraction.

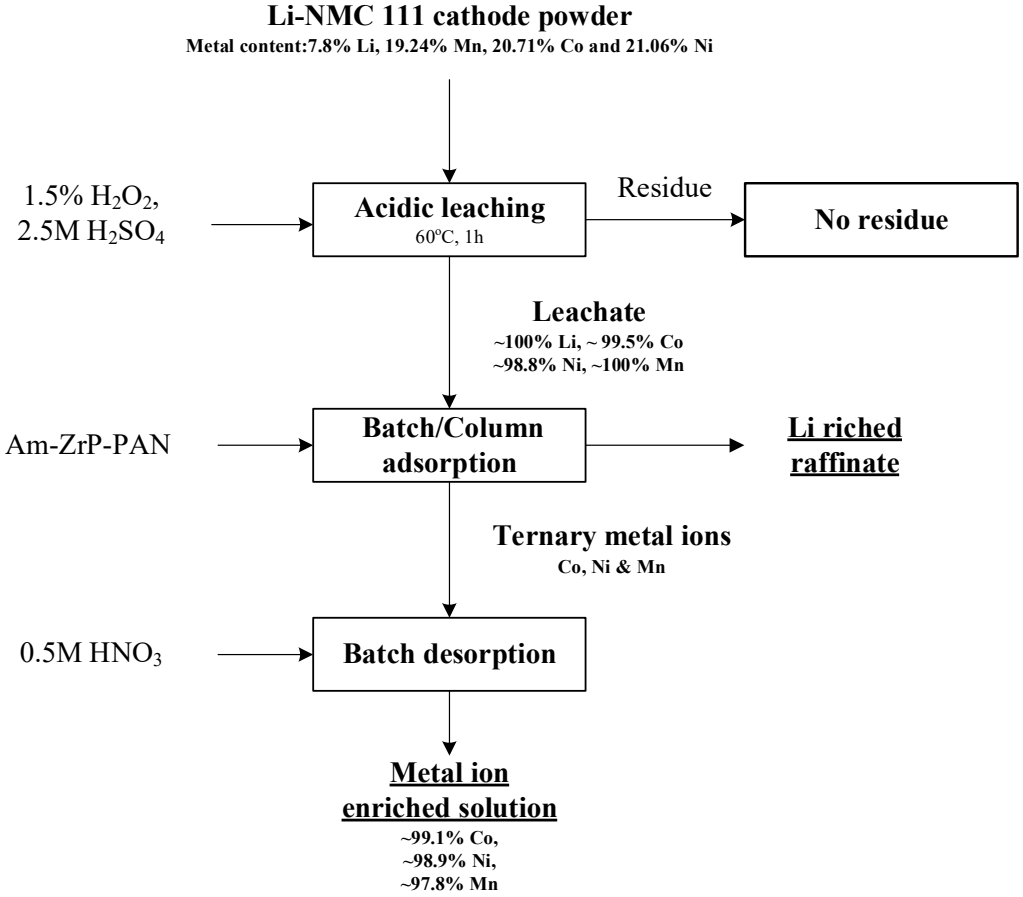

Figure 6. Mass flow scheme for metal recovery from NMC 111 cathode powder from end-of-life lithium-ion batteries.

4. Conclusions

In summary, transition metals can be effectively separated from lithium with am-ZrP/PAN. The optimal leaching conditions were determined to be a pulp density of 40 g/L, H_2O_2 concentration of 1.5%, H_2SO_4 concentration of 2.5 M, temperature of 60 °C, and leaching time of 60 min. Under these experimental conditions, the leaching efficiencies for Li, Co, Ni, Mn, and Co were 99.9%, 99.5%, 98.9%, and 99.9%, respectively. In batch sorption, am-ZrP/PAN favors the metal ions Co, Ni, and Mn over Li, which indicates high selectivity towards the divalent ions. The isothermal data for am-ZrP/PAN followed pseudo-second-order kinetic models, with a theoretical maximum sorption of 0.045, 0.037, and 0.095 mmol g^{-1} for Co, Ni, and Mn, respectively, corresponding to the experimental maximum sorption, which indicates that the adsorption mechanism was chemical adsorption. In addition, the desorption theoretical data indicated a high metal ion recovery of 99.1% Co, 98.9% Ni, and 97.8% Mn. The results of the column loading/stripping experiment corresponded with those of the batch sorption experiment. The loading process demonstrated selectivity for Li over Co, Ni, and Mn, indicating that Li separation could be achieved. For the stripping, highly pure Mn and Ni were separated using 0.1 M H_3PO_4 and 0.5 M HNO_3, respectively. Compared with traditional solvent extraction processes, not only can this method help to simplify the process for recovering transition metals from spent LIBs, but it could also reduce the use of highly toxic solvents. However, as the adsorption capacity of am-ZrP/PAN is still low, further investigation to improve this capacity is much needed for industrial applications.

Author Contributions: B.H.: Writing—original draft, methodology, investigation. Z.L.: Methodology and investigation. J.T.: Validation, investigation, writing—review and editing, methodology. J.K.: Writing—review and editing, methodology. R.K.: Writing—review and editing. M.A.M.: Writing—review and editing. H.B.: Funding acquisition, methodology, writing—review and editing. J.X.: Conceptualization, methodology, supervision, writing—review and editing. All authors have read and agreed to the published version of the manuscript.

Funding: This research was funded by the Chinese Academy of Sciences Pioneer "Hundred Talents Program" Young Talents (Class C), the European Community's Seventh Framework Programme ([FP7/2007-2013]) under grant agreement [607411] and the RAMI infrastructure project with grant number [293109].

Data Availability Statement: The data presented in this study are available on request from the corresponding author. The data are not publicly available due to privacy.

Acknowledgments: The research leading to these results received funding from the Chinese Academy of Sciences Pioneer "Hundred Talents Program" Young Talents (Class C) and the European Community's Seventh Framework Programme ([FP7/2007-2013]) under grant agreement no. 607411 (MC-ITN EREAN: European Rare Earth Magnet Recycling Network). This publication reflects only the authors' views, exempting the Community from any liability. X-ray tomography was funded by the Research Council of Finland via the RAMI infrastructure project (#293109).

Conflicts of Interest: The authors declare no conflict of interest.

References

1. Manthiram, A. A reflection on lithium-ion battery cathode chemistry. *Nat. Commun.* **2020**, *11*, 1550. [CrossRef]
2. Harper, G.; Sommerville, R.; Kendrick, E.; Driscoll, L.; Slater, P.; Stolkin, R.; Walton, A.; Christensen, P.; Heidrich, O.; Lambert, S.; et al. Recycling lithium-ion batteries from electric vehicles. *Nature* **2019**, *575*, 75–86. [CrossRef]
3. Tarascon, J.M.; Armand, M. Issues and challenges facing rechargeable lithium batteries. *Nature* **2001**, *414*, 359–367. [CrossRef] [PubMed]
4. Wagner, A.C.; Bohn, N.; Geßwein, H.; Neumann, M.; Osenberg, M.; Hilger, A.; Manke, I.; Schmidt, V.; Binder, J.R. Hierarchical Structuring of NMC111-Cathode Materials in Lithium-Ion Batteries: An In-Depth Study on the Influence of Primary and Secondary Particle Sizes on Electrochemical Performance. *ACS Appl. Energy Mater.* **2020**, *3*, 12565–12574. [CrossRef]
5. Nitta, N.; Wu, F.; Lee, J.T.; Yushin, G. Li-ion battery materials: Present and future. *Mater. Today* **2015**, *18*, 252–264. [CrossRef]
6. Shaju, K.M.; Bruce, P.G. Macroporous $Li(Ni_{1/3}Co_{1/3}Mn_{1/3})O_2$: A high-rate positive electrode for rechargeable lithium batteries. *J. Power Sources* **2007**, *174*, 1201–1205. [CrossRef]
7. Dunn, J.B.; Gaines, L.; Kelly, J.C.; James, C.; Gallagher, K.G. The significance of Li-ion batteries in electric vehicle life-cycle energy and emissions and recycling's role in its reduction. *Energy Environ. Sci.* **2015**, *8*, 158–168. [CrossRef]
8. Genchi, G.; Carocci, A.; Lauria, G.; Sinicropi, M.S.; Catalano, A. Nickel: Human Health and Environmental Toxicology. *Int. J. Environ. Res. Public Health* **2020**, *17*, 679. [CrossRef]
9. Leyssens, L.; Vinck, B.; Van Der Straeten, C.; Wuyts, F.; Maes, L. Cobalt toxicity in humans-A review of the potential sources and systemic health effects. *Toxicology* **2017**, *387*, 43–56. [CrossRef]
10. Kang, D.H.P.; Chen, M.; Ogunseitan, O.A. Potential Environmental and Human Health Impacts of Rechargeable Lithium Batteries in Electronic Waste. *Environ. Sci. Technol.* **2013**, *47*, 5495–5503. [CrossRef]
11. Olivetti, E.A.; Ceder, G.; Gaustad, G.G.; Fu, X. Lithium-Ion Battery Supply Chain Considerations: Analysis of Potential Bottlenecks in Critical Metals. *Joule* **2017**, *1*, 229–243. [CrossRef]
12. Bae, H.; Kim, Y. Technologies of lithium recycling from waste lithium ion batteries: A review. *Mater. Adv.* **2021**, *2*, 3234–3250. [CrossRef]
13. Roy, J.J.; Cao, B.; Madhavi, S. A review on the recycling of spent lithium-ion batteries (LIBs) by the bioleaching approach. *Chemosphere* **2021**, *282*, 130944. [CrossRef] [PubMed]
14. Zheng, X.; Zhu, Z.; Lin, X.; Zhang, Y.; He, Y.; Cao, H.; Sun, Z. A Mini-Review on Metal Recycling from Spent Lithium Ion Batteries. *Engineering* **2018**, *4*, 361–370. [CrossRef]
15. Meshram, P.; Pandey, B.D.; Mankhand, T.R. Extraction of lithium from primary and secondary sources by pre-treatment, leaching and separation: A comprehensive review. *Hydrometallurgy* **2014**, *150*, 192–208. [CrossRef]
16. Chagnes, A.; Pospiech, B. A brief review on hydrometallurgical technologies for recycling spent lithium-ion batteries. *J. Chem. Technol. Biotechnol.* **2013**, *88*, 1191–1199. [CrossRef]
17. Sahu, S.; Agrawala, M.; Patra, S.R.; Devi, N. Synergistic Approach for Selective Leaching and Separation of Strategic Metals from Spent Lithium-Ion Batteries. *ACS Omega* **2024**, *9*, 10556–10565. [CrossRef] [PubMed]
18. Xuan, W.; de Souza Braga, A.; Korbel, C.; Chagnes, A. New insights in the leaching kinetics of cathodic materials in acidic chloride media for lithium-ion battery recycling. *Hydrometallurgy* **2021**, *204*, 105705. [CrossRef]

19. Meshram, P.; Virolainen, S.; Abhilash; Sainio, T. Solvent Extraction for Separation of 99.9% Pure Cobalt and Recovery of Li, Ni, Fe, Cu, Al from Spent LIBs. *Metals* **2022**, *12*, 1056. [CrossRef]
20. Chen, X.; Chen, Y.; Zhou, T.; Liu, D.; Hu, H.; Fan, S. Hydrometallurgical recovery of metal values from sulfuric acid leaching liquor of spent lithium-ion batteries. *Waste Manag.* **2015**, *38*, 349–356. [CrossRef]
21. Provazi, K.; Campos, B.A.; Espinosa, D.C.R.; Tenório, J.A.S. Metal separation from mixed types of batteries using selective precipitation and liquid–liquid extraction techniques. *Waste Manag.* **2011**, *31*, 59–64. [CrossRef] [PubMed]
22. Choubey, P.K.; Dinkar, O.S.; Panda, R.; Kumari, A.; Jha, M.K.; Pathak, D.D. Selective extraction and separation of Li, Co and Mn from leach liquor of discarded lithium ion batteries (LIBs). *Waste Manag.* **2021**, *121*, 452–457. [CrossRef] [PubMed]
23. Wang, W.-Y.; Yen, C.H.; Lin, J.-L.; Xu, R.-B. Recovery of high-purity metallic cobalt from lithium nickel manganese cobalt oxide (NMC)-type Li-ion battery. *J. Mater. Cycles Waste Manag.* **2019**, *21*, 300–307. [CrossRef]
24. Chen, W.-S.; Ho, H.-J. Recovery of Valuable Metals from Lithium-Ion Batteries NMC Cathode Waste Materials by Hydrometallurgical Methods. *Metals* **2018**, *8*, 321. [CrossRef]
25. Wang, F.; Sun, R.; Xu, J.; Chen, Z.; Kang, M. Recovery of cobalt from spent lithium ion batteries using sulphuric acid leaching followed by solid–liquid separation and solvent extraction. *RSC Adv.* **2016**, *6*, 85303–85311. [CrossRef]
26. Huang, B.; Pan, Z.; Su, X.; An, L. Recycling of lithium-ion batteries: Recent advances and perspectives. *J. Power Sources* **2018**, *399*, 274–286. [CrossRef]
27. Davis, K.; Demopoulos, G.P. Hydrometallurgical recycling technologies for NMC Li-ion battery cathodes: Current industrial practice and new R&D trends. *RSC Sustain.* **2023**, *1*, 1932–1951. [CrossRef]
28. Alvial-Hein, G.; Mahandra, H.; Ghahreman, A. Separation and recovery of cobalt and nickel from end of life products via solvent extraction technique: A review. *J. Clean. Prod.* **2021**, *297*, 126592. [CrossRef]
29. Yao, Y.; Zhu, M.; Zhao, Z.; Tong, B.; Fan, Y.; Hua, Z. Hydrometallurgical Processes for Recycling Spent Lithium-Ion Batteries: A Critical Review. *ACS Sustain. Chem. Eng.* **2018**, *6*, 13611–13627. [CrossRef]
30. Yang, Y.; Xu, S.; He, Y. Lithium recycling and cathode material regeneration from acid leach liquor of spent lithium-ion battery via facile co-extraction and co-precipitation processes. *Waste Manag.* **2017**, *64*, 219–227. [CrossRef]
31. Liu, P.; Xiao, L.; Tang, Y.; Zhu, Y.; Chen, H.; Chen, Y. Resynthesis and electrochemical performance of $LiNi_{0.5}Co_{0.2}Mn_{0.3}O_2$ from spent cathode material of lithium-ion batteries. *Vacuum* **2018**, *156*, 317–324. [CrossRef]
32. Lei, S.; Cao, Y.; Cao, X.; Sun, W.; Weng, Y.; Yang, Y. Separation of lithium and transition metals from leachate of spent lithium-ion batteries by solvent extraction method with Versatic 10. *Sep. Purif. Technol.* **2020**, *250*, 117258. [CrossRef]
33. Xu, J.; Wiikinkoski, W.E.; Koivula, R.; Zhang, W.; Ebin, B.; Harjula, R. HF-free synthesis of a-zirconium phosphate and its use as ion exchanger for separation of Nd(III) and Dy(III) from a ternary Co–Nd–Dy system. *J. Sustain. Metall.* **2017**, *3*, 646–658. [CrossRef]
34. Poole, C.F.; Yu, L.; Sun, Y. Chapter 1—Concepts and milestones in the development of ion-exchange chromatography. In *Ion-Exchange Chromatography and Related Techniques*; Nesterenko, P.N., Poole, C.F., Sun, Y., Eds.; Elsevier: Amsterdam, The Netherlands, 2024; pp. 1–23.
35. Wiikinkoski, W.E.; Xu, J.; Zhang, W.; Hietala, S.; Koivula, T.R. Modification of α-zirconium phosphate synthesis—Effects of crystallinity and acidity on Eu(III) and Am(III) ion exchange. *ChemistrySelect* **2018**, *3*, 9583–9588. [CrossRef]
36. Wang, H.; Huang, K.; Zhang, Y.; Chen, X.; Jin, W.; Zheng, S.; Zhang, Y.; Li, P. Recovery of Lithium, Nickel, and Cobalt from Spent Lithium-Ion Battery Powders by Selective Ammonia Leaching and an Adsorption Separation System. *ACS Sustain. Chem. Eng.* **2017**, *5*, 11489–11495. [CrossRef]
37. Strauss, M.L.; Diaz, L.A.; McNally, J.; Klaehn, J.; Lister, T.E. Separation of cobalt, nickel, and manganese in leach solutions of waste lithium-ion batteries using Dowex M4195 ion exchange resin. *Hydrometallurgy* **2021**, *206*, 105757. [CrossRef]
38. Virolainen, S.; Wesselborg, T.; Kaukinen, A.; Sainio, T. Removal of iron, aluminium, manganese and copper from leach solutions of lithium-ion battery waste using ion exchange. *Hydrometallurgy* **2021**, *202*, 105602. [CrossRef]
39. Xu, J.; Virolainen, S.; Zhang, W.; Kuva, J.; Sainio, T.; Koivula, R. Polyacrylonitrile-encapsulated amorphous zirconium phosphate composite adsorbent for Co, Nd and Dy separations. *Chem. Eng. J.* **2018**, *351*, 832–840. [CrossRef]
40. Xu, J.; Koivula, R.; Zhang, W.; Wiikinkoski, E.; Hietala, S.; Harjula, R. Separation of cobalt, neodymium and dysprosium using amorphous zirconium phosphate. *Hydrometallurgy* **2018**, *175*, 170–178. [CrossRef]
41. Ma, F.; Shi, W.; Meng, H.; Li, Z.; Zhou, W.; Zhang, L. Preparation, characterization and ion-exchange behavior of polyantimonic acid-polyacrylonitrile (PAA–PAN) composite beads for strontium(II). *J. Radioanal. Nucl. Chem.* **2016**, *308*, 155–163. [CrossRef]
42. He, L.-P.; Sun, S.-Y.; Mu, Y.-Y.; Song, X.-F.; Yu, J.-G. Recovery of Lithium, Nickel, Cobalt, and Manganese from Spent Lithium-Ion Batteries Using l-Tartaric Acid as a Leachant. *ACS Sustain. Chem. Eng.* **2017**, *5*, 714–721. [CrossRef]
43. He, L.-P.; Sun, S.-Y.; Song, X.-F.; Yu, J.-G. Leaching process for recovering valuable metals from the $LiNi_{1/3}Co_{1/3}Mn_{1/3}O_2$ cathode of lithium-ion batteries. *Waste Manag.* **2017**, *64*, 171–181. [CrossRef] [PubMed]